Method to measure off-axis displacements based on the analysis of the intensity distribution of a vortex beam

G. Anzolin,* F. Tamburini, A. Bianchini, and C. Barbieri
Dipartimento di Astronomia, Università di Padova, vicolo dell'Osservatorio 3, I-35122 Padova, Italy
(Received 2 January 2009; published 30 March 2009)

We study the properties of the Fraunhofer diffraction patterns produced by Gaussian beams crossing spiral phase plates. We show, both analytically and numerically, that off-axis displacements of the input beam produce asymmetric diffraction patterns. The intensity profile along the direction of maximum asymmetry shows two different peaks. We find that the intensity ratio between these two peaks decreases exponentially with the off-axis displacement of the incident beam, the decay being steeper for higher strengths of the optical singularity of the spiral phase plate. We analyze how this intensity ratio can be used to measure small misalignments of the input beam with a very high precision.

DOI: 10.1103/PhysRevA.79.033845 PACS number(s): 42.25.Bs, 42.25.Gy, 42.90.+m, 42.79.−e

I. INTRODUCTION

Optical vortices (OVs) appear in light beams carrying screw wave-front dislocations (vortex beams) [1]. The surface of constant phase of a vortex beam has an helical structure and presents phase singularities endowed with topological charge. Beams harboring OVs carry also a quantity of orbital angular momentum (OAM) [2] associated to the precession of the Poynting vector around the vortex axis [3].

OVs have attracted an increasing interest in applied physics [4–9] and also for astronomical applications [10–15]. In fact, they can be easily produced in light beams with the help of specific optical devices that have a central optical singularity. Among these optical elements, the most efficient ones are fork holograms (FHs) [16] and spiral phase plates (SPPs) [17]. Laguerre-Gaussian (L-G) modes have been often used to describe the beams produced with such devices. However, a more precise description of the diffraction patterns produced by an SPP [18] or a FH [19,20] is provided by hypergeometric (Kummer) functions. We shall use this approach in this paper.

Consider an input beam with an amplitude distribution symmetric about the propagation axis. When such a beam intersects an SPP or a FH perpendicularly and exactly on axis, it produces a circularly symmetric beam with a central dark region, where the field amplitude is zero. Any misalignment with respect to the central discontinuity would then produce an asymmetry of the observed intensity distribution [21] and the topological charge of the correspondent off-axis OV may have a noninteger value [22]. This changes also the OAM originally carried by the beam [23], thus producing an OAM spectrum [24,25].

The sensitivity of a vortex beam to displacements of the input beam has been proposed as an indicator of nanometric shifts in a speckle pattern [26] or to be used as a noninterferometric method for the correction of small surface deviations on spatial light modulators [27]. Similar results could be obtained from the analysis of the mean-square value of the resulting OAM spectrum [28]. We also proposed a method to measure very small displacements based on the degree of asymmetry of the intensity pattern of an off-axis vortex beam [13,29]. However, detailed analytical studies of the actual structure of off-axis OV produced with SPPs of FHs were initiated only very recently [30]. In this paper, we extend the analysis of the intensity distribution of an off-axis vortex beam generated under Fraunhofer diffraction conditions. We then derive a more convenient formalism of our method for the detection of off-axis displacements, in view of future applications with optical imaging devices.

II. FRAUNHOFER DIFFRACTION OF A GAUSSIAN BEAM INTERSECTING A SPIRAL PHASE PLATE ON AXIS

In this section we revisit the problem of the Fraunhofer diffraction of a monochromatic Gaussian beam intersecting an SPP exactly on axis [31]. The geometrical configuration adopted here is sketched in Fig. 1. The SPP is placed in the (x,y) plane and the central optical singularity coincides with

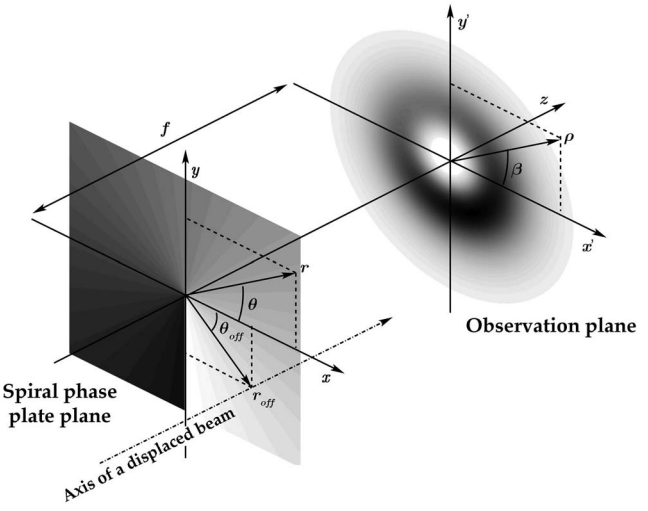

FIG. 1. The geometrical configuration adopted to study the Fraunhofer diffraction of a Gaussian beam beyond a spiral phase plate (see text for details).

*Also at INAF-Osservatorio Astronomico di Capodimonte, salita Moiariello 16, I-80131 Napoli, Italy; gabriele.anzolin@unipd.it

the origin of the (x,y) coordinate system. To take advantage of the circular symmetry of the geometry, in the following we will use the circular coordinates (r,θ) defined by $x=r\cos\theta$ and $y=r\sin\theta$. Thus, the transmission function of the SPP is a complex function of the azimuthal angle θ,

$$T_\ell(\theta)=e^{i\ell\theta}, \tag{1}$$

where ℓ represents the strength of the optical singularity. We consider a Gaussian beam propagating along the z axis (that is also its symmetry axis) perpendicular to the SPP plane. This choice is important for practical applications, i.e., laser beams or starlight beams affected by atmospheric turbulence. We then assume that the field amplitude distribution in the SPP plane is

$$A_G(r)=ce^{-r^2/w^2}, \tag{2}$$

where c is a complex factor, eventually dependent on the z coordinate, and w is related to the beam width. The observation plane (x',y') is located at a distance $f\to\infty$ beyond the SPP or, better, at the focal plane of a lens placed just behind the SPP (in this case, f would coincide with the focal length of the lens). The scalar field of the beam in the observation plane can be obtained from the Fourier transform of the product between the amplitude of the input beam and the SPP transmission function,

$$u_\ell(\rho,\beta)=\text{const}\int\int A_G(r)T_\ell(\theta)e^{-ikr\rho\cos(\theta-\beta)/f}rdrd\theta, \tag{3}$$

where $k=2\pi/\lambda$ is the wave vector, λ is the wavelength, and (ρ,β) are the circular coordinates in the observation plane. To simplify the calculations, the SPP is considered as infinitely extended in the (x,y) plane. In addition, we use the scaled radial coordinate $r'=kr/f$ and introduce the quantities $w_0=f/(kw)$ and c_0, the latter containing all the multiplicative constants. In this way, Eq. (3) becomes

$$u_\ell(\rho,\beta)=c_0\int_0^{2\pi}\int_0^\infty e^{-w_0^2r'^2}e^{i\ell\theta}e^{-ir'\rho\cos(\theta-\beta)}r'dr'd\theta. \tag{4}$$

The integral involving the angular coordinate θ can be evaluated by using the definition of the Bessel function of the first kind $J_n(z)$. Thus, the integral involving the spatial coordinate becomes a particular case of the Weber-Sonine formula [32]. The final result of the integration can be expressed in terms of the confluent hypergeometric function of the first kind. However, a more useful expression of the amplitude distribution of the output beam is obtained by using the modified Bessel function of the first kind $I_\nu(z)$. By introducing the quantity $\eta=\rho/(2w_0)$, the final result is [19]

$$u_\ell(\rho,\beta)=c_0i^{-\ell}\frac{\pi^{3/2}}{2w_0^2}e^{i\ell\beta}e^{-\eta^2/2}\eta\left[I_{(\ell-1)/2}\left(\frac{\eta^2}{2}\right)-I_{(\ell+1)/2}\left(\frac{\eta^2}{2}\right)\right]. \tag{5}$$

The presence of the phase factor $e^{i\ell\beta}$ implies that the output beam has an ℓ-charged OV nested inside.

Beams of this kind, also known as "Kummer beams" [20], are different from the commonly used Laguerre-Gaussian beams [33,34]. If $\ell=0$, the Bessel functions of half-integer index in Eq. (5) can be expressed in terms of the hyperbolic functions and combined together to give an exponential. In this case, the amplitude distribution of the output beam is still Gaussian, i.e., $u_0\sim e^{-\eta^2}$. If $\ell\neq0$, we can derive a useful approximation for $\eta\to0$ by using the series expansion of $I_\nu(z)$ [32],

$$I_\nu(z)=\left(\frac{z}{2}\right)^\nu\sum_{m=0}^{\infty}\frac{(z/2)^{2m}}{m!\,\Gamma(\nu+m+1)}. \tag{6}$$

We can recognize that, near the z axis, the amplitude of an on-axis Kummer beam carrying an OV with topological charge ℓ could be represented by a superposition of amplitudes of L-G modes with $p=0$,

$$u_\ell\sim e^{-\eta^2/2}\eta^\ell\left[\frac{1}{\Gamma\left(\frac{\ell+1}{2}\right)}-\frac{\eta^2}{2^2\Gamma\left(\frac{\ell+3}{2}\right)}+\frac{\eta^4}{2^4\Gamma\left(\frac{\ell+3}{2}\right)}-\frac{\eta^6}{2^6\Gamma\left(\frac{\ell+5}{2}\right)}+\mathcal{O}(\eta^8)\right]. \tag{7}$$

The dominant term is represented by an L-G mode with index ℓ, while higher order terms are L-G modes with indices $\ell+2m$ $(m=1,2,\ldots)$.

A. Properties of the intensity distribution

The intensity distribution of an on-axis Kummer beam is axially symmetric around the z axis and is described by

$$I_\ell(\rho,\beta)\approx|u_\ell(\rho,\beta)|^2=c_0^2\frac{\pi^3}{4w_0^4}e^{-\eta^2}\eta^2\left[I_{(\ell-1)/2}\left(\frac{\eta^2}{2}\right)-I_{(\ell+1)/2}\left(\frac{\eta^2}{2}\right)\right]^2. \tag{8}$$

As for L-G modes, the intensity pattern of a Kummer beam has an annular shape, with a central dark region where the intensity is zero. However, there are some fundamental differences between the two analytical descriptions. For a Kummer beam the behavior of the intensity at large distances from the z axis is $\sim\eta^{-4}$, while for an L-G mode it decreases exponentially. Moreover, the radius of maximum intensity of an L-G mode is $\rho_{\max}\sim\sqrt{\ell/2}$, where the intensity attains the value $I(\rho_{\max})\sim\ell^\ell e^{-\ell}/\ell!$, while for a Kummer beam $\rho_{\max}$ is found by numerically solving the transcendental equation,

$$(\ell+2\eta^2)I_{(\ell+1)/2}\left(\frac{\eta^2}{2}\right)+(\ell-2\eta^2)I_{(\ell-1)/2}\left(\frac{\eta^2}{2}\right)=0. \tag{9}$$

The calculation of the radii of maximum intensity obtained for a set of values of the topological charge $\ell=0,1,\ldots,10$ [see Fig. 2(a)] suggests that $\rho_{\max}$ is linearly dependent on ℓ,

$$\frac{\rho_{\max}}{2w_0}=(0.37\pm0.01)+(0.470\pm0.002)\ell. \tag{10}$$

A similar result was found also for OVs produced by a plane wave intersecting a finite circular phase mask [6]. Figure

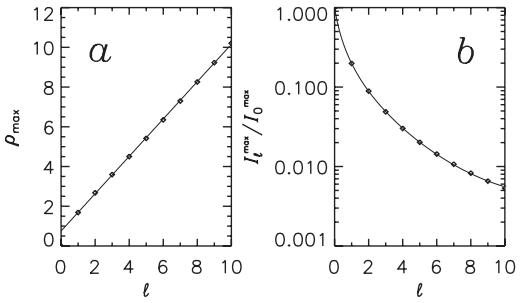

FIG. 2. Properties of the intensity distribution of on-axis Kummer beams having $\ell=0,1,\ldots,10$. (a) Plot of the radius of maximum intensity $\rho_{\max}$ (in units of w_0) vs ℓ. (b) Plot of the intensity calculated at $\rho_{\max}$ for different values of ℓ. The maximum intensity for $\ell=0$ has been set to unity.

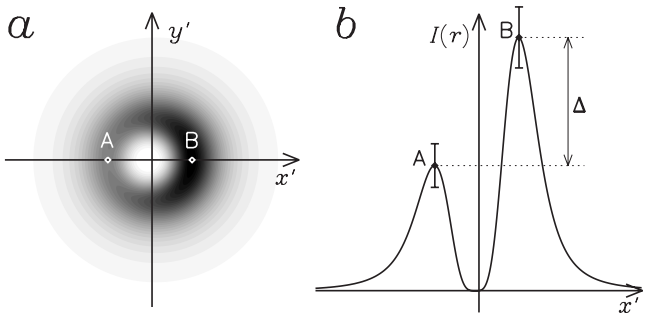

FIG. 3. Example of the far-field intensity pattern of a numerically simulated off-axis vortex beam produced by an $\ell=2$ SPP. The two diamonds indicate the positions of the two different intensity peaks A and B. (a) Contour plot of the intensity distribution obtained in the observation plane. (b) Intensity profile of the off-axis beam extracted along the x' direction. Δ is the difference between the intensities calculated in B and A. Examples of error bars are reported for both the intensity peaks (see text).

2(b) shows the intensity calculated at $\rho_{\max}$ for the same set of topological charges.

B. Effects of off-axis displacements

When the input Gaussian beam is displaced off axis, so that its symmetry axis does not coincide with the z axis of Fig. 1, the intensity pattern produced in the observation plane is modified. The misalignment of the input beam can be decomposed into a translation in the (x,y) plane and an inclination angle ω with respect to the z axis. However, if ω is small, the modifications induced in the intensity pattern of the output beam are negligible [30]. For this reason, in our calculations we will consider only lateral displacements of the incident beam. Let us then assume that the Gaussian beam intersects the SPP in the position $(r_{\text{off}},\theta_{\text{off}})$, as shown in Fig. 1. The field of the output beam resembles that of Eq. (5) obtained under on-axis conditions,

$$u_\ell(\rho,\beta)=c_0 i^{-\ell}\frac{\pi^{3/2}}{2w_0^2}e^{i\ell\psi}e^{-w_0^2 r_{\text{off}}'^2}e^{-\gamma^2/8w_0^2}\frac{\gamma}{2w_0}\times\left[I_{(\ell-1)/2}\left(\frac{\gamma^2}{8w_0^2}\right)-I_{(\ell+1)/2}\left(\frac{\gamma^2}{8w_0^2}\right)\right]. \quad (11)$$

Here, r'_{off} is the scaled radial coordinate obtained from r_{off}, while the quantities γ and ψ are defined as [30],

$$\begin{cases}\gamma^2=\rho^2+4iw_0^2 r'_{\text{off}}\rho\cos(\beta-\theta_{\text{off}})-4w_0^4 r'^2_{\text{off}}\\ \tan\psi=\dfrac{\rho\sin\beta+2iw_0^2 r'_{\text{off}}\sin\theta_{\text{off}}}{\rho\cos\beta+2iw_0^2 r'_{\text{off}}\cos\theta_{\text{off}}}\end{cases}. \quad (12)$$

In this case, the additional exponential factor and the complex value of γ^2 produces a phase singularity which is located neither on the beam axis, nor in the origin of the (x',y') plane, but shifted in a position $(\rho,\beta)=(2w_0^2 r'_{\text{off}},\theta_{\text{off}}+\pi/2)$. As a result, the intensity distribution of the output beam becomes asymmetric [35], showing two different peaks along the direction of the vortex core in the (x',y') plane. Figure 3(a) shows an example of an off-axis OV produced with an $\ell=2$ SPP. The lower and the higher peaks are labeled with A and B, respectively.

Now, since it is difficult to find analytical solutions of Eqs. (11) and (12), we decided to perform numerical simulations. The width w of the input Gaussian beam was parametrized in function of the full width at half of the intensity maximum, $2a$, such that $a=w\sqrt{\ln 2/2}$. We used values of the topological charge induced by the SPP in the range $\ell=0,1,\ldots,10$, since with higher values we get misleading results using the two-dimensional fast Fourier transform algorithm. For each ℓ, we considered a number of off-axis displacements r_{off}/a of the input beam ranging from 0 to 1 and computed the intensity patterns of the resulting beams.

We checked the consistency of our numerical simulations by comparing them to the analytical models [Eq. (11)] for a number of values of ℓ and off-axis positions. To this aim, we previously normalized the intensities of both the simulated and the analytical patterns to the corresponding maximum values. Therefore, the B peak always has a normalized intensity equal to one (obviously, both the peaks A and B will have the same unity intensity if $r_{\text{off}}/a=0$). The residuals of the subtraction of the theoretical intensity patterns from the simulated ones are typically within 10^{-4} for positions close to peaks A and B. We will then assume this quantity as the intrinsic error of our numerical simulations.

For all the numerically simulated OVs we obtained the intensity values at the two peaks and calculated the quantity R defined as the ratio between the intensity I_A of the lower peak and the intensity I_B of the higher peak. We find that R rapidly decreases as the off-axis displacement increases for all the topological charges considered. The graphs showing the dependence of R on r_{off}/a for $\ell=1,2,3,4,5$ are plotted in Fig. 4. All the curves are well represented by a simple exponential function,

$$R=k_1 e^{-k_2 r_{\text{off}}/a}, \quad (13)$$

where parameters k_1 and k_2, obtained by best fitting the simulated curves, are listed in Table I. From these results, it appears that k_2 depends on the topological charge ℓ as

$$k_2=(4.64\pm0.05)-(2.9\pm0.2)e^{-(0.47\pm0.05)\ell}, \quad (14)$$

while k_1 seems to remain equal to unity.

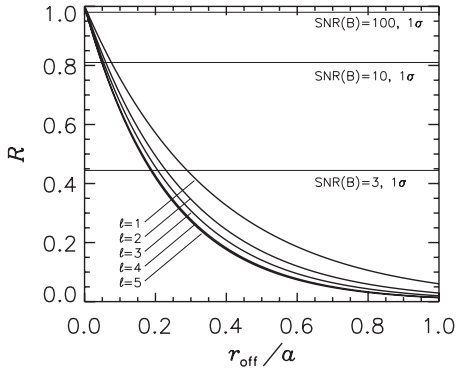

FIG. 4. Plot of the peaks intensity ratio R vs the off-axis displacement of the input Gaussian beam obtained for different values of the topological charge induced by the SPP. Horizontal lines are drawn at the maximum values of R detectable at the 1σ confidence level for three values of the SNR of the B peak.

III. SENSITIVITY OF THE METHOD TO REVEAL OFF-AXIS DISPLACEMENTS

The off-axis displacement of the input Gaussian beam with respect to the central singularity of an SPP results in an asymmetry of the far-field intensity pattern. Equation (13) reveals that the parameter R represents an extremely sensitive tool to detect such very small displacements.

Let us suppose to have an input Gaussian beam which symmetry axis is perpendicular to the surface of an SPP and observe the correspondent far-field image with a photoelectric detector such as a charge-coupled device. In this way, if the beam is displaced off axis, we can measure the intensity ratio R of the two different peaks, as defined in Sec. II B. The precision of this measurement is mainly limited by the signal-to-noise ratio (SNR) achieved in the observation, while additional errors might be introduced by construction imperfections of the SPP. The latter issue results in inhomogeneities of the observed intensity distribution. For this reason, efforts are currently made to improve the production quality of SPPs [36–38]. However, here we assume to use an ideal SPP so that the only limitations are due to the SNR.

TABLE I. Best-fit values of parameters k_1 and k_2 in Eq. (13) obtained from least-square fits of the simulated curves of Fig. 4. The associated errors are given at the 1σ confidence level.

ℓ	k_1	k_2
1	1.002 ± 0.001	2.808 ± 0.006
2	1.0012 ± 0.0007	3.534 ± 0.004
3	1.0004 ± 0.0005	3.928 ± 0.003
4	0.9995 ± 0.0008	4.259 ± 0.005
5	0.9990 ± 0.0009	4.338 ± 0.006
6	0.999 ± 0.001	4.432 ± 0.008
7	0.998 ± 0.001	4.456 ± 0.008
8	0.998 ± 0.001	4.509 ± 0.009
9	0.998 ± 0.001	4.573 ± 0.01
10	0.998 ± 0.002	4.756 ± 0.02

The noise of a CCD detector is mainly represented by the photon shot noise [39]. Assuming a pure Poissonian distribution of the collected photons, the uncertainties associated to the intensities I_A and I_B of the two peaks can be approximated by the square root of the signals, i.e., $\sigma_A = \sqrt{I_A}$ and $\sigma_B = \sqrt{I_B}$. We may then recognize $I_A \neq I_B$ at the $n\sigma$ confidence level when $\Delta = I_B - I_A \geq n\sigma_A + n\sigma_B$ [see Fig. 3(b)], that means

$$\Delta \geq n(\sqrt{I_A} + \sqrt{I_B}). \tag{15}$$

If we introduce parameter R, this equation can be rewritten as a function of the only SNR associated to the intensity of the highest peak $[R_{SN}(B)]$. We find that the maximum peak intensity ratio measurable at the $n\sigma$ confidence level is

$$R \leq \left(1 - \frac{n}{R_{SN}(B)}\right)^2. \tag{16}$$

As useful examples, in Fig. 4 we draw three horizontal lines corresponding to the maximum R values 0.44, 0.81, and 0.98 detectable at the 1σ level for $R_{SN}(B) = 3$, 10, and 100, respectively. By combining Eq. (13) with Eq. (16), we finally obtain the expression for the minimum off-axis displacement detectable at the $n\sigma$ confidence level,

$$\frac{r_{off}}{a} \geq -\frac{1}{k_2} \ln\left[\frac{1}{k_1}\left(1 - \frac{n}{R_{SN}(B)}\right)^2\right]. \tag{17}$$

One general outcome is that, for a fixed $R_{SN}(B)$, OVs with higher ℓ values allow the detection of smaller off-axis displacements. This effect is more significant at low SNR regimes, when the maximum measurable R is small and the curves in Fig. 4 are more spatially separated. As $R_{SN}(B)$ increases, the advantage obtained by using high values of the topological charge becomes negligible. In fact, if we assume $R_{SN}(B)$ above 10, we might reveal off-axis displacements $<0.1a$ for all ℓ values. Instead, considering the lowest acceptable value $R_{SN}(B) = 3$ for signal detection, we can detect off-axis displacements of $\sim 0.3a$ for $\ell = 1$ at the 1σ confidence level.

IV. CONCLUSIONS

In this paper we have analyzed the properties of the Fraunhofer diffraction pattern produced by a Gaussian light beam crossing an SPP. When the input beam is perfectly aligned with the central singularity of the SPP, the resulting beam is a Kummer beam with a symmetric annular intensity distribution. Instead, an off-axis displacement of the input beam produces an asymmetry in the far-field intensity pattern. In particular, the intensity profile along the direction of maximum asymmetry shows two different peaks. We have found that, for all the values of the topological charge considered, the ratio R of their intensities changes exponentially with the off-axis displacement of the input beam. We have quantitatively analyzed how the SNR associated to the highest peak affects the sensitivity of the ratio R in revealing very small misalignments of the input beam. In particular, we have found that higher values of the topological charge ℓ generally provide better resolutions, especially for low SNR regimes. We suggest that this method could find interesting

applications in high-precision positioning systems. Note that similar results can be obtained also by using other spatial properties of transverse laser modes [40]. Finally, the sensitivity of OVs could be used in astrometry by placing an SPP at the focal plane of a telescope.

ACKNOWLEDGMENT

We gratefully acknowledge financial support from the CARIPARO foundation.

[1] J. F. Nye and M. V. Berry, Proc. R. Soc. London, Ser. A **336**, 165 (1974).
[2] L. Allen, M. W. Beijersbergen, R. J. C. Spreeuw, and J. P. Woerdman, Phys. Rev. A **45**, 8185 (1992).
[3] M. J. Padgett and L. Allen, Opt. Commun. **121**, 36 (1995).
[4] K. T. Gahagan and G. A. Swartzlander, Jr., Opt. Lett. **21**, 827 (1996).
[5] G. Molina-Terriza, J. Recolons, J. P. Torres, L. Torner, and E. M. Wright, Phys. Rev. Lett. **87**, 023902 (2001).
[6] J. E. Curtis and D. G. Grier, Phys. Rev. Lett. **90**, 133901 (2003).
[7] D. G. Grier, Nature (London) **424**, 810 (2003).
[8] I. G. Mariyenko, J. Strohaber, and C. J. Uiterwaal, Opt. Express **13**, 7599 (2005).
[9] G. Molina-Terriza, J. P. Torres, and L. Torner, Nat. Phys. **3**, 305 (2007).
[10] G. A. Swartzlander, Jr., Opt. Lett. **26**, 497 (2001).
[11] M. Harwit, Astrophys. J. **597**, 1266 (2003).
[12] B. Thidé, H. Then, J. Sjöholm, K. Palmer, J. Bergman, T. D. Carozzi, Y. N. Istomin, N. H. Ibragimov, and R. Khamitova, Phys. Rev. Lett. **99**, 087701 (2007).
[13] G. Anzolin, F. Tamburini, A. Bianchini, G. Umbriaco, and C. Barbieri, Astron. Astrophys. **488**, 1159 (2008).
[14] N. M. Elias II, Astron. Astrophys. **492**, 883 (2008).
[15] G. C. G. Berkhout and M. W. Beijersbergen, Phys. Rev. Lett. **101**, 100801 (2008).
[16] V. Y. Bazhenov, M. V. Vasnetsov, and M. S. Soskin, JETP Lett. **52**, 429 (1990).
[17] M. W. Beijersbergen, R. P. C. Coerwinkel, M. Kristensen, and J. P. Woerdman, Opt. Commun. **112**, 321 (1994).
[18] M. V. Berry, J. Opt. A, Pure Appl. Opt. **6**, 259 (2004).
[19] Z. S. Sacks, D. Rozas, and G. A. Swartzlander, Jr., J. Opt. Soc. Am. B **15**, 2226 (1998).
[20] A. Y. Bekshaev and A. I. Karamoch, Opt. Commun. **281**, 1366 (2008).
[21] A. Vaziri, G. Weihs, and A. Zeilinger, J. Opt. B: Quantum Semiclassical Opt. **4**, S47 (2002).
[22] S. S. R. Oemrawsingh, E. R. Eliel, G. Nienhuis, and J. P. Woerdman, J. Opt. Soc. Am. A Opt. Image Sci. Vis **21**, 2089 (2004).
[23] A. Mair, A. Vaziri, G. Weihs, and A. Zeilinger, Nature (London) **412**, 313 (2001).
[24] M. V. Vasnetsov, J. P. Torres, D. V. Petrov, and L. Torner, Opt. Lett. **28**, 2285 (2003).
[25] M. V. Vasnetsov, V. A. Pas'ko, and M. S. Soskin, New J. Phys. **7**, 46 (2005).
[26] W. Wang, T. Yokozeki, R. Ishijima, M. Takeda, and S. G. Hanson, Opt. Express **14**, 10195 (2006).
[27] A. Jesacher, A. Schwaighofer, S. Fürhapter, C. Maurer, S. Bernet, and M. Ritsch-Marte, Opt. Express **15**, 5801 (2007).
[28] Y.-D. Liu, C. Gao, X. Qi, and H. Weber, Opt. Express **16**, 7091 (2008).
[29] F. Tamburini, G. Anzolin, G. Umbriaco, A. Bianchini, and C. Barbieri, Phys. Rev. Lett. **97**, 163903 (2006).
[30] A. Y. Bekshaev and A. I. Karamoch, Opt. Commun. **281**, 3597 (2008).
[31] Similar results can be found also for a FH, provided that the angle subtended by the first diffraction order is small [20].
[32] M. Abramowitz and I. A. Stegun, *Handbook of Mathematical Functions with Formulas, Graphs, and Mathematical Tables* (Dover, New York, 1964).
[33] G. A. Turnbull, D. A. Robertson, G. M. Smith, L. Allen, and M. J. Padgett, Opt. Commun. **127**, 183 (1996).
[34] J. Arlt, K. Dholakia, L. Allen, and M. J. Padgett, J. Mod. Opt. **45**, 1231 (1998).
[35] I. V. Basistiy, V. A. Pas'ko, V. V. Slyusar, M. S. Soskin, and M. V. Vasnetsov, J. Opt. A, Pure Appl. Opt. **6**, S166 (2004).
[36] S. S. R. Oemrawsingh, J. A. W. van Houwelingen, E. R. Eliel, J. P. Woerdman, E. J. K. Verstegen, J. G. Kloosterboer, and G. W. 't Hooft, Appl. Opt. **43**, 688 (2004).
[37] T. Watanabe, M. Fujii, Y. Watanabe, N. Toyama, and Y. Iketaki, Rev. Sci. Instrum. **75**, 5131 (2004).
[38] K. Sueda, G. Miyaji, N. Miyanaga, and M. Nakatsuka, Opt. Express **12**, 3548 (2004).
[39] S. B. Howell, *Handbook of CCD astronomy*, 2nd ed. (Cambridge University Press, Cambridge, United Kingdom, 2006) Vol. 5.
[40] N. Treps, N. Grosse, W. P. Bowen, C. Fabre, H.-A. Bachor, and P. K. Lam, Science **301**, 940 (2003).